Opto-Electronic Engineering

Article

2017, Vol 44, Issue 8

High-precision measurement of low reflectivity specular object based on phase measuring deflectometry

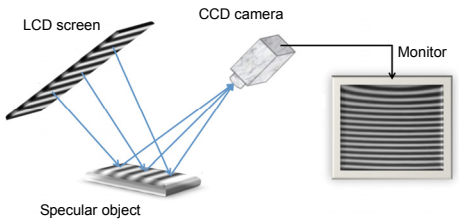

Yuxiang Wu, Huimin Yue* and Yong Liu

State Key Laboratory of Electronic Thin Films and Integrated Devices, School of Optoelectronic Information, University of Electronic Science and Technology of China, Chengdu 610054, China

Abstract: Phase measuring deflectometry (PMD) is a robust, noncoherent technique for the characterization of specular surface. For measuring high specular reflectivity surface, PMD can deliver micron radian range local gradient. However, when the measured surface has low specular reflectivity, the accuracy of the measured gradient is low since the captured fringe pattern shows low signal to noise ratio. The phase error characteristics in PMD system when testing low reflectivity surfaces are analyzed. The analysis illustrates that the random phase error increases rapidly while the nonlinear error drops slowly with the decreasing of the tested surface reflectivity. In order to attain high precision measurement of low reflectivity specular surface, a robust error reduction method based on wavelet de-noising is proposed to reduce the phase error. This error reduction method is compared with several other normally used methods in both simulation and experiment work. The method based on the wavelet de-noising shows better performance when measuring the low reflectivity specular surface.

Keywords: phase measuring deflectometry; fringe reflection; optical three-dimentional measurement; phase error analysis

DOI: 10.3969/j.issn.1003-501X.2017.08.002 **Citation:** *Opto-Elec Eng*, 2017, **44**(8): 772–780

1 Introduction

The three-dimensional (3D) metrology for specular reflecting surfaces attracts much attention due to their various applications in optics, electronics, or semiconductor industries. Phase measuring deflectometry (PMD) [1-3] is an effective tool to measure the specular surface gradient information. Further evaluation can deliver the curvature or height of the test surface.

The high sensitivity of PMD allows measuring gradient changes in the range of micro-scale and local height changes in the range of nanometers[4,5]. This technique is suitable for solving the nowadays measurement problems in the automobiles industry when high precision inspection of surfaces and defects is required[6]. PMD is also an ideal method for inspection or qualification of the eyeglass and machined high-quality surface components surfaces.

Received 12 May 2017; accepted 18 July 2017
* E-mail: yuehuimin@uestc.edu.cn

However, the accuracy of the PMD is related to the phase reliability of the captured fringe pattern. Errors in the phase map influence the accuracy of the whole measurement. When testing low reflectivity specular surfaces like cell phone shell, contrast of the distorted fringe patterns is very low, and there are always relatively big errors in the phase map.

Fig. 1(a) is the distorted fringe pattern of a typical mobile shell captured in PMD experiments. Fig. 1(b) is the wrapped phase map retrieved from the captured fringe pattern. Fig. 1(c) is the middle row of Fig. 1(a). The quality of the fringe pattern is low. As a contrast, Figs. 1(d), 1(e)~1(f) are the fringe pattern and the wrapped phase of a high reflectivity surface. In comparison with the high reflectivity surface, the low reflectivity surface suffers much more errors in the phase map. Therefore, a robust error reduction method is required to reach high precision measurement of surface. As far as the authors know, error analyzing and reduction when measuring low reflectivity surface in PMD was seldom discussed before. In this paper, errors characteristics of the low reflectivity specular surface are discussed, and a robust de-noising method based on wavelet de-noising is discussed.

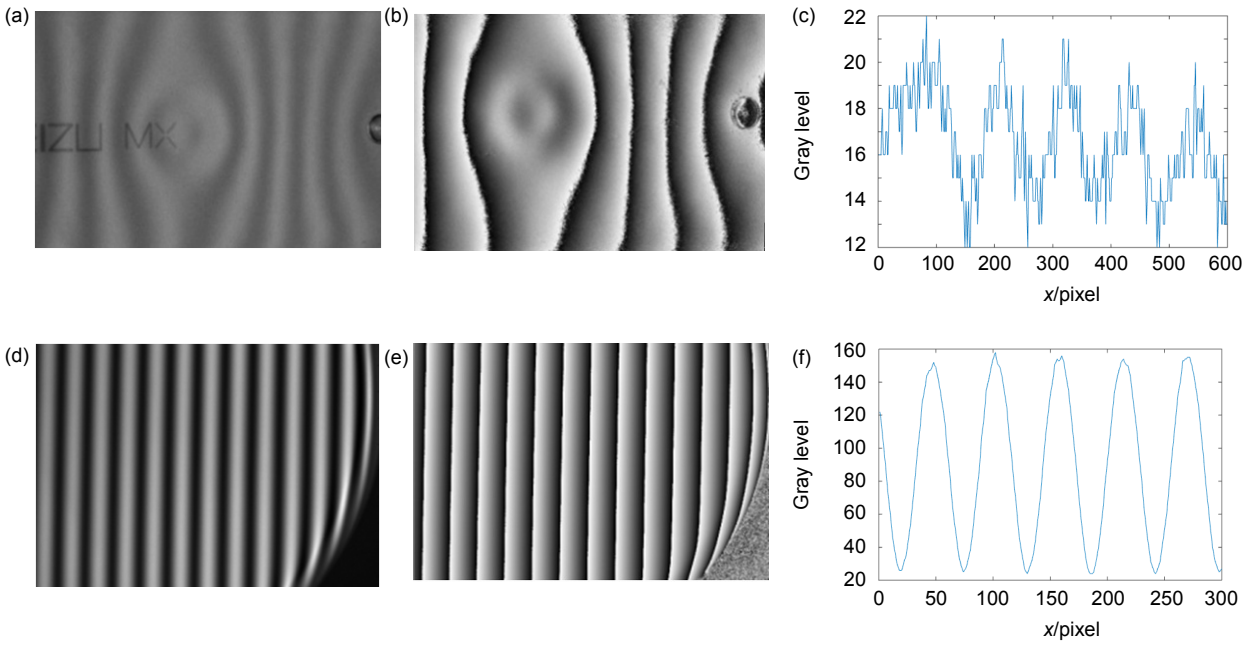

Fig. 1 Comparison of the fringe patterns of low and high reflectivity surfaces. (a) The distorted fringe pattern of a low reflectivity surface. (b) The wrapped phase map of the low reflectivity surface. (c) Middle row of (a). (d) The distorted fringe pattern of a high reflectivity surface. (e) The wrapped phase map of the high reflectivity surface. (f) Middle row of (d).

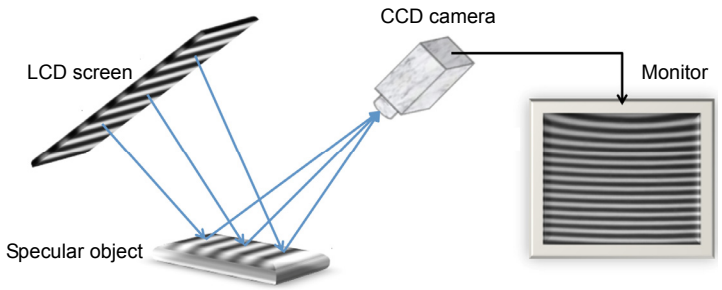

Fig. 2 Schematic setup of PMD.

This article is arranged as follows. In section 2, analysis of error characteristics in measuring low reflectivity surface by PMD is carried out. Sections 3 and 4 discuss a de-noising method based on wavelet transform. Section 5 shows the experimental work and section 6 concludes the work.

2 Analysis of error characteristics of low reflectivity specular surface

Fig. 2 shows the arrangement of the PMD. The generated phase-shifting fringe patterns in x and y directions with an equal spacing period P are displayed on a liquid crystal display (LCD) screen. The CCD camera records the distorted fringe patterns reflected by the specular surface.

Equation (1) shows the expression of ideal captured distorted fringe pattern in x direction.

$$I(x,y)=A(x,y)+B(x,y)\cdot\cos(\varphi(x,y)), \quad (1)$$

where $I(x,y)$ is the recorded intensity, x and y are spatial coordinates, A and B are the background and modulation intensities, and A has a larger mean value than B. $\varphi(x,y)$ is the phase including the carrier phase and gradient-related phase. Then, the surface shape is reconstructed from gradient.

The random error and the nonlinear error are two important errors in fringe projection profilometry[7-10], as well as in PMD. The nonlinear error is usually larger than the random error[11,12]. The nonlinear responses of LCD and CCD camera are the main nonlinear error sources, and the nonlinear response of LCD screen plays a bigger role[9,13].

The random error and nonlinear error for low reflec-

tivity specular surface are analyzed.

2.1 Random error

Electronic noise of the CCD camera is the main random error source, and the electronic noise can be simplified as a kind of signal independent random noise which is additive and Gaussian[14-16].

With the random noise, the captured x direction fringe pattern distribution will be:

$$I_r(x,y) = A(x,y) + B(x,y)\cdot\cos(\varphi(x,y)) + E_r(x,y) \quad , \quad (2)$$

where $E_r(x,y)$ is the random noise with a mean value of zero and a nonzero standard deviation. Simulation was taken to find the relationship between the phase error and background intensity A as well as modulation intensity B. For simple analysis, A and B didn't change with spatial coordinates x and y. The random noise $E_r(x,y)$ was added to each fringe pattern and $E_r(x,y)$ had the standard deviation of 0.3. Four-step phase shifting method was taken to extract the phase. A and B were changed separately. B is set to be 5 (unit: gray level) and A varies from 5 to 100 (unit: gray level). As a result, in Fig. 3(a), the error in the unwrapped phase does not change much with A, which means the background light intensity does not influence the random error in the unwrapped phase.

The relation between B and phase error is shown in Fig. 3(b), and A is set to be 100. The phase error is sensitive to the modulation intensity. The error in the phase becomes very big when B is smaller than 30.

In Fig. 1(c), B has the value of 10, and Fig. 1(f) of 65. The root mean square (RMS) of the random phase error with low reflectivity surface is 10 times larger than that with high reflectivity surface in Fig. 1. The value of B is related to the reflectivity of the tested surface. Low reflectivity leads to a very small B in the captured fringe pattern. So, a robust random error reduction method must be taken into account in the measurement of low reflectivity surface.

2.2 Nonlinear error

The response functions of the LCD display and CCD camera [10,13] are the main nonlinear error source in PMD. In consideration of the 5-order harmonics nonlinear, the captured x direction fringe pattern distribution is changed to Eq. (3)[10,17]:

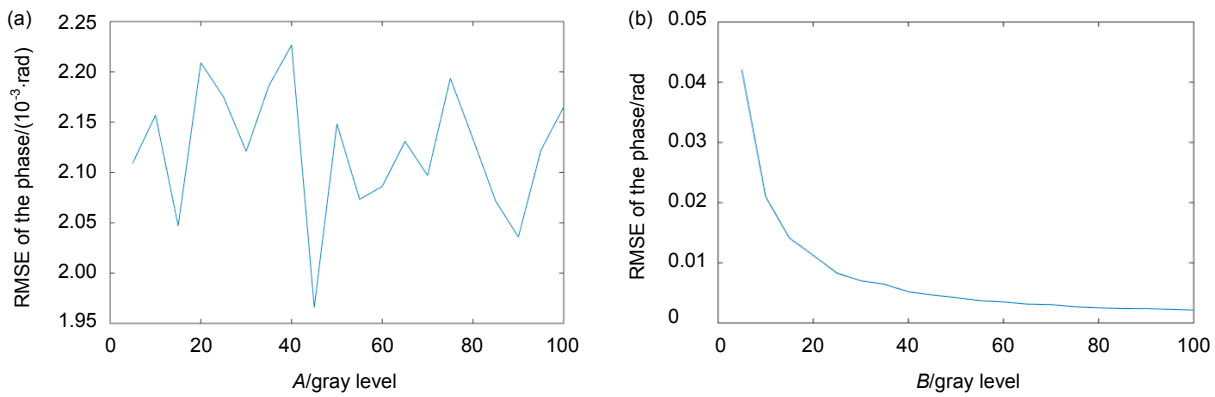

Fig. 3 Relation between the random phase error. (a) Background intensity A. (b) Modulation intensity B.

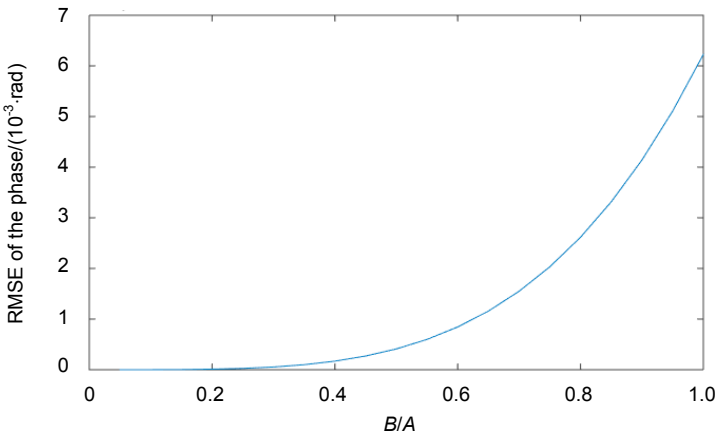

Fig. 4 Relation between B/A and nonlinear error.

$$I_n(x,y) = I(x,y) + aI^2(x,y) + bI^3(x,y) + cI^4(x,y) + dI^5(x,y) \ , \quad (3)$$

In the simulation, a, b, c and d are 0.05^2, 0.01^3, 0.001^4 and 0.001^5, respectively. The nonlinear error in the phase increases with the rise of B/A. The result is shown in Fig. 4(a), in which A is 100 and B/A changes from 0.05 to 1. Therefore, the RMS of the nonlinear phase error of high reflectivity is bigger than that in low reflectivity surface in Fig. 1.

In short, in comparison with high reflectivity surface, there is a big random error in the phase map when measuring a low reflectivity surface, yet the nonlinear error is smaller.

3 Error reduction methods in PMD

The least square temporal phase unwrapping (TPU) [10, 18] method can be used to reduce random phase error in PMD. In the least square TPU, a computer generates fringe patterns with time-varying spatial frequencies. The phase unwrapping is conducted along the pixel history instead of spatial direction. Intermediate phase values are used to improve the accuracy of final unwrapped phase value. However, the least square TPU methods need plenty of fringe patterns, and thus require a lot of shooting time.

As an excellent signal processing method, wavelet de-noising has been introduced into many signal-processing fields. In fringe projection profilometry, for the goal of achieving an accurate dynamic measurement, the wavelet transform method has been used as a single frame projecting method (which is called as wavelet transform profilometry) [19-21] to extract phase map from the distorted fringe pattern. At the same time, it can also decrease random errors. This attempt failed because of the relatively long processing time (normally more than 100 seconds for a 1000×1000 resolution figure) [20]. In addition, extracting the phase from a single fringe pattern based on Fourier methods (Fourier transform, windowed Fourier transform and wavelet transform) brings in theoretical phase errors unless compensations are taken. Nevertheless, wavelet transform technique is an excellent random noise reduction method (a few seconds processing time) in the image processing field [22, 23]. In this paper we use distorted fringe pattern as a phase extracting method, and the wavelet transform can be used as a de-noising method to reduce the random error on the phase map in PMD.

Among the common nonlinear removal methods [11, 12, 17, 24], the phase shifting method is the most simple and robust. 6-step phase shifting class B method in Ref. [17] can erase the influence of 5-order harmonics, which is enough for most situations. Combined the 6-step phase shifting with the de-noise characteristic of wavelet transform, an effective method (we call it extended PMD) is proposed in this paper to decrease the nonlinear error and the large random error simultaneously. The method is executed by the following steps:

1) Generate fringe patterns on the display LCD screen;

2) Record the distorted fringe patterns through the specular surface by CCD camera;

3) Demodulate the wrapped phase by 6-step phase shifting method to reduce the nonlinear error at the same time;

4) Unwrap the phase and get the two directions slope-related phase distribution;

5) Reduce the random error by wavelet de-noising method;

6) Get the two directions slope distributions. Calculate the curvature distributions by the derivation of slopes and reconstruct the height by the integral of slopes.

4 Simulation

Simulations are taken to see the performance of the above steps in reducing errors. The simulations are divided into three sections: overall error reduction performance, comparison with least-square TPU and influence of wavelet de-noising on the PMD phase details.

4.1 The error reduction performance

In the simulation, the tested object is a plane. 5-order harmonics and random noise (the value is similar to the experiment data) are added to each fringe pattern. The nonlinear error expression is Eq. (3), and the coefficients a, b, c and d are 0.02^2, 0.002^3, 0.0001^4 and 0.0001^5, respectively. The random noise is assumed to be from -2.5 to 2.5 and the standard deviation is assumed to be 1.44. The wavelet function "sym3" is used in the wavelet transform method. The middle row of the phase map without error reduction method and the phase map with the method based on wavelet de-noising (extended PMD) described above is compared in Fig. 5(a). The simulations prove that the wavelet de-noising has an excellent error reduction effect for low reflectivity surface measurement in PMD.

Another simulation is carried out to show which one works better, wavelet transform directly on the fringe pattern or on phase map. The result is shown in Fig. 5(b) and the error reduction effect is better with the wavelet de-noising on the phase map.

4.2 Comparison of the wavelet de-noising with least-square TPU

In TPU, the unwrapped phase quality is dominated by the smallest wavelength fringe pattern quality. The least-square TPU method has a good random error reduction effect with a relatively large number of captured fringe patterns. Simulation is taken to compare the effect of the wavelet de-noising method (extended PMD) with linear sequence least-square TPU method. In the simulation, the tested object was a plane, and random noise with the range from -5 to 5 and the standard deviation 2.89 was added on each fringe pattern. The maximum

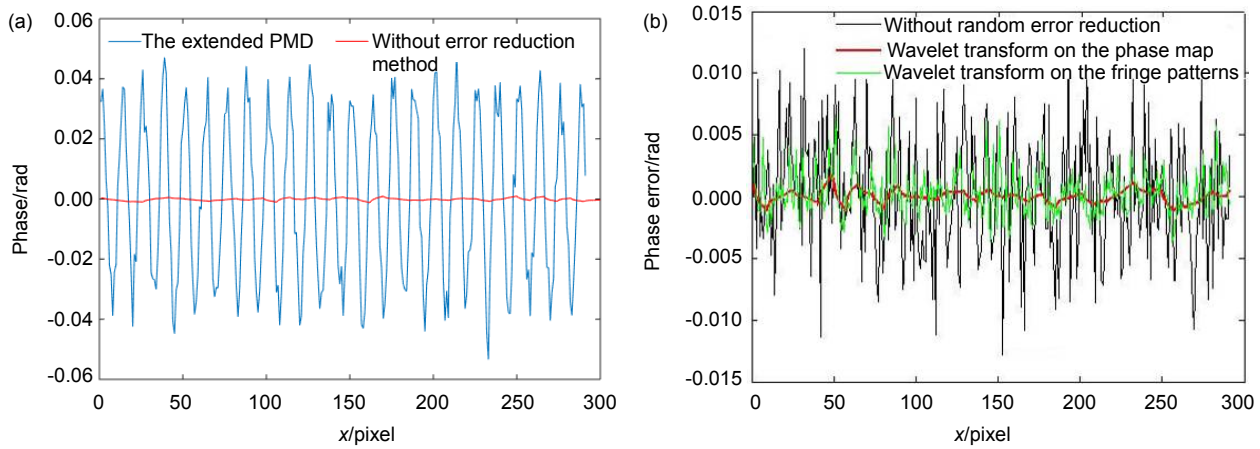

Fig. 5 Error reduction performance. (a) Error reduction result. (b) Comparison of the wavelet de-noising effect work on the fringe pattern and the unwrapped phase.

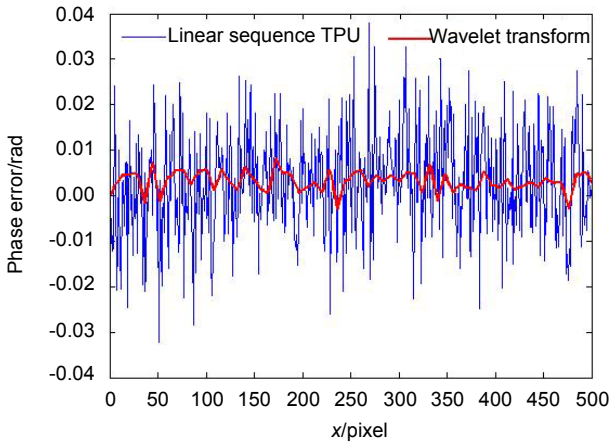

Fig. 6 Comparison results of wavelet de-noising method and linear sequence TPU in reducing random error.

spatial frequency of the fringe pattern in least-square TPU was 8. Comparison results of the middle lines of the phase maps with the two methods are shown in Fig. 6. It is seen that the wavelet de-noising has better random error reduction ability than linear sequence least-square TPU method.

4.3 The influence of wavelet de-noising on the phase distortions in PMD

In this section, we are trying to find optimal parameters of wavelet transform for de-noising, while at the same time, protect the phase distortions and details. In addition, a comparison with the commonly used random error reduction method (low-pass Gaussian filter) is given.

A phase map with different kinds of distortions (including conical, step-like and spherical distortions) is generated in a computer simulation, as shown in Fig. 7(a). The random error, with the range from -0.2 rad to +0.2 rad (similar to the random error in low reflectivity surface measurement experiment) is added to the phase map.

Several parameters are analyzed in order to get a good random error reduction effect. Three important parameters are the mother wavelet function, the level of decomposition and the thresholding method[25]. Here, the error reduction performance of Fig. 7(a) is the evaluation standard for choosing the most suitable parameters.

For the selection of mother wavelet function, only the orthogonal wavelets (Daubechies, Coiflect and Symlet families) are in consideration since the orthogonal wavelet transform is relatively concise and requires less processing time. The Daubechies 1~9 wavelets, Symlet 1~9 wavelets and Coiflect 1~5 wavelets are simulated to process on Fig. 7(a). Except Symlet 1 and Daubechies 1 wavelets, which damage larger in the useful signal than others, other wavelets have similar error reduction capability. Fig. 7(b) shows the data of the red line in Fig. 7(a)

after the process of Symlet 5 wavelet de-noising. Fig. 7(c) is the residual error(compared with the correct phase signal) after the process of Symlet 5 wavelet de-noising. The top of conical phase distortion is slightly damaged by wavelet de-noising. The absolute error here is only 4% (0.06/1.5) of the original signal and 30% (0.06/0.2) of the added random error. However, the edges of other distortions are not influenced. Other parameters in this simulation include 'soft' thresholding, 'rigrsure' thresholding rule and the decomposition level is 5.

The capability of the wavelet transform in suppressing the random error rises with the decomposition level in our simulation, but this capability increases slightly when the decomposition level is higher than 5. However, the damage to the correct phase distortions also increases with the decomposition level. Therefore, the 5 decomposition level is the most suitable for the noise situation like Fig. 7(a).

There are two common thresholding methods (soft and hard) and four common thresholding rules (Rigrsure, Sqtwolog, Heursure and Minimaxi). Hard thresholding sets the components whose values are smaller than the threshold to zero. The soft thresholding also has this rule, but the soft thresholding makes the nonzero coefficients shrinking gradually to zero. Normally, the soft thresholding has the better performance than hard thresholding since the hard thresholding may cause discontinuities in the thresholding signal around the thresholding value[25]. The rigrsure thresholding rule behaves the best in remaining the original signal in our simulation. While in the capability of suppressing the random error, the order is Sqtwolog (the RMS error compared with the correct phase is 0.057473), Heursure(RMS error 0.057476), Minimaxi (RMS error 0.057479) and Rigrsure (RMS error 0.057500), but their differences are small. So, the optimal parameters for our experiment will be 5 decomposition level, 'soft' thresholding and 'rigrsure' thresholding rule. The wavelet function has many choices as discussed above.

Fig. 7(d) gives the data of red line in Fig. 7(a) after the process of the common used low-pass Gaussian filter. The Gaussian window size is 10×10 and the standard deviation is 5. Fig. 7(e) shows the residual error. There are damages at the edges of the step-like phase distortion, and the absolute error in these places is over 40% of the original signal (the wavelet de-noising is 4%). Though Fig. 7(e) looks much smoother than Fig. 7(c), the random error in the normal position has the similar range. The increase of window size can reduce more random errors, but this will also cause more damage to discontinuous

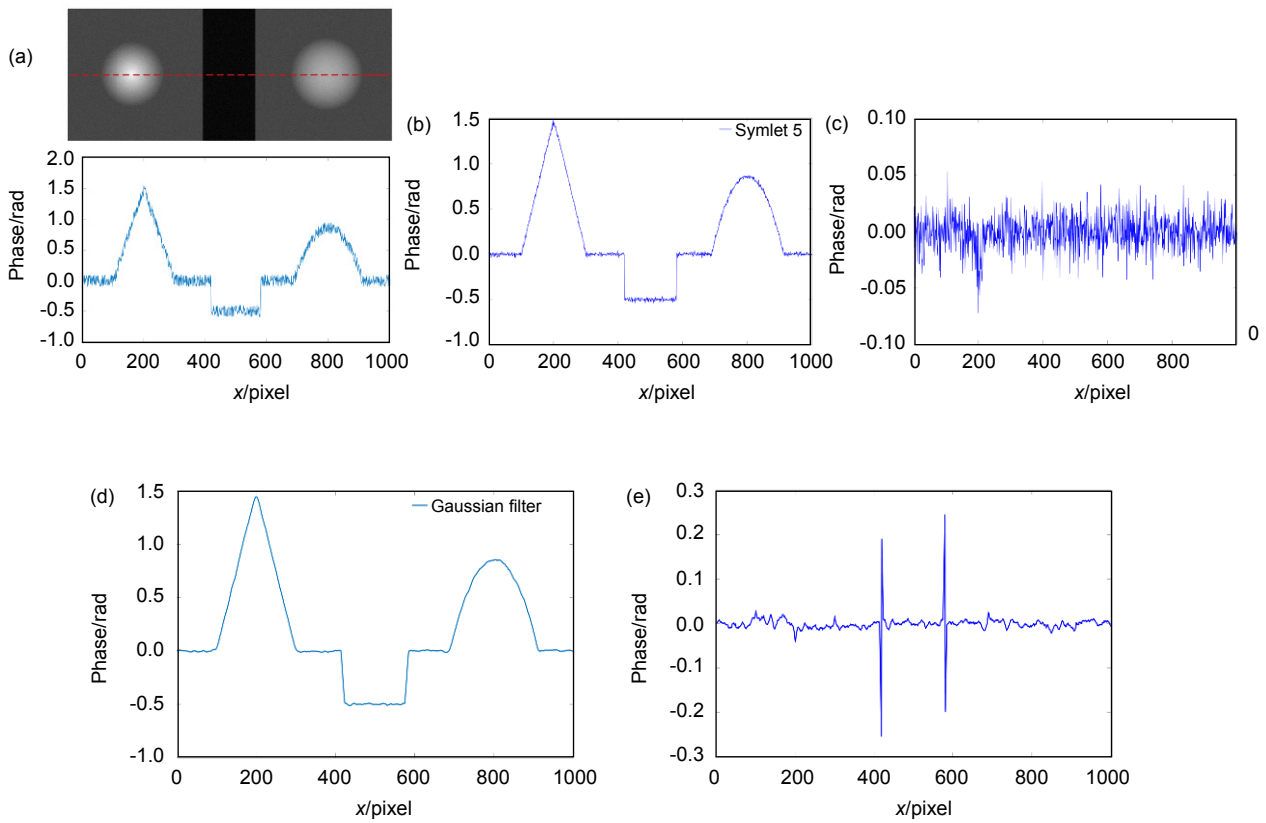

Fig. 7 The simulation results of the wavelet parameter selection and low-pass Gaussian filter de-noising. (a) The noisy phase. (b) The data of red line in (a) after the process of Symlet 5 wavelet de-noising. (c) The residual error of wavelet de-noising. (d) The data of red line after a low-pass Gaussian filter. (e) The residual error of Gaussian filter de-noising.

phase distortion.

In conclusion, the method based on wavelet de-noising has an excellent performance in decreasing the errors and the details on the phase map are barely destroyed. So, in our simulation, when compared to the least-square TPU method, the method based on wavelet de-noising needs much less shooting time and has a more outstanding error reduction effect. In comparison with the low-pass Gaussian filter method, the wavelet de-noising method performs better in the preservation of phase details.

5 Experiment

Measurement setup of the experiment is shown in Fig. 8. The hardware system is composed of a CCD camera (Manta G-125B/C) and LCD screen. A 50 mm focal length lens is used in camera (Computar M5018-MP2).

A typical mobile shell is measured. The system spatial

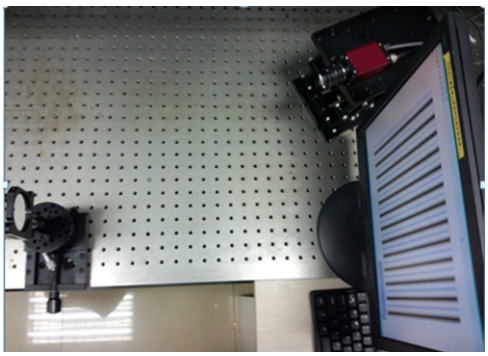

Fig. 8 Setup of the experiment.

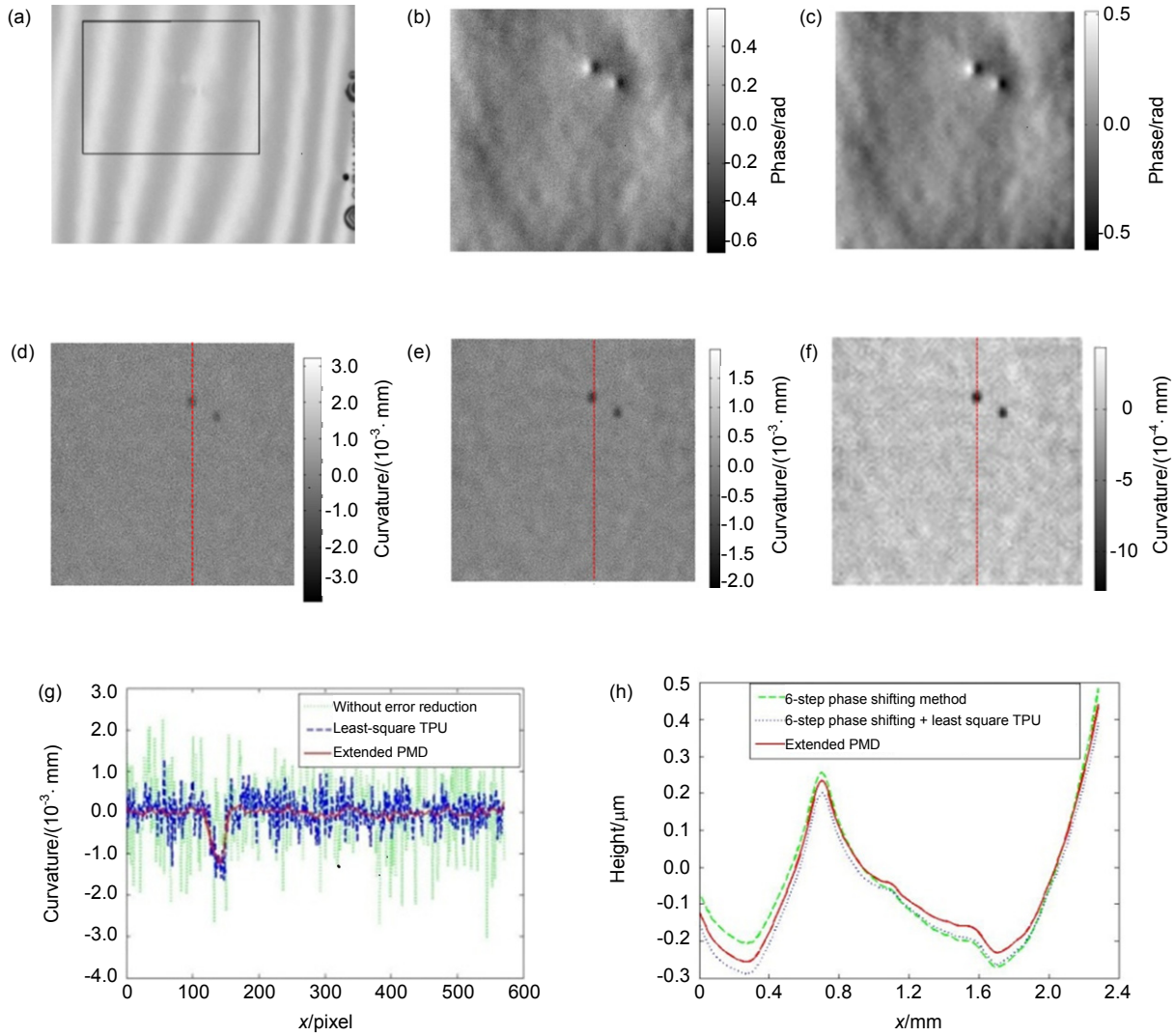

Fig. 9 The experimental results of the mobile shell. (a) The tested mobile shell. (b), (c) The *x*-direction phase distribution without error reduction and with the method based on wavelet de-noisings(extended PMD). (d)~(f) The curvature distribution without error reduction, with least-square TPU method, and with the method described in the manuscript, respectively. (g) The data of red lines in (d)~(f). (h) The lines of the reconstructed height distribution with no error reduction, with least-square TPU method, and with the method described in the manuscript, respectively.

resolution is about 40 microns. Three methods (without error reduction, least-square TPU, and the method based on wavelet de-noisings) are employed to measure mobile shell curvature (the derivation of the slope) and height. The linear sequence least-square TPU is combined with 6-step phase shifting method. Fig. 9(a) shows a distorted fringe pattern and the rectangle area denotes the processed region. Figs. 9(b) and 9(c) are the extracted phase distributions without error reduction and with the method based on wavelet de-noising, from which the good performance of the method based on wavelet de-noising in reducing nonlinear and random errors is demonstrated.

Figs. 9(d)~(f) show the measured curvature when employing the three error reduction methods respectively. Fig. 9(g) shows the data of lines in Figs. 9(d)~(f). It is shown that the method based on wavelet de-noising performs the best in improving the measurement accuracy.

Fig. 9(h) illustrates the lines in the height distribution of the three methods in the same position with Fig. 9(g). It should be noted that in order to show the results clearly, the low-frequency surface shape has been removed in each figure. The method based on wavelet de-noising (extended PMD) and the least-square TPU have the similarly reconstructed height results. The reason is the integration technique (least-square integration method with Southwell grid model was used) used in the height reconstruction process suppressed the random error in some degree. While in the situation without the error reduction, the defects on the cell phone shell can hardly be detected and the reconstructed height contains big error.

In some situations, if the curvature maps are required for the inspection of defects, especially when the tested surfaces have low reflectivity, the method based on wavelet de-noising would be quite suitable for error reduction.

The method based on wavelet de-noising is also suitable to detect small defects and for the measurement of the high reflective surface to reach higher precision. Fig. 10(a) shows the distorted fringe pattern of a plane mirror. Fig. 10(b) is the phase map of the denoted region in Fig. 10(a) by the method based on wavelet de-noising(extended PMD). Fig. 10(c) gives the comparison of the data on the red line of Fig. 10(b) with the data in the same position of the phase map by using only 6-step phase shifting method. The RMS phase error with the method based on wavelet de-noising is 5 times smaller than that with only 6-step phase shifting method.

6 Conclusions

The low reflectivity specular surface leads to big phase errors in phase measuring deflectometry (PMD). A robust error reduction method is required in order to achieve high precision measurement. In this paper, the error characteristic for low reflectivity specular surface is analyzed. For measuring the low reflectivity specular surface, the random phase error increases a lot and the nonlinear error decreases a little. A method based on wavelet de-noising is proposed to improve the measure-

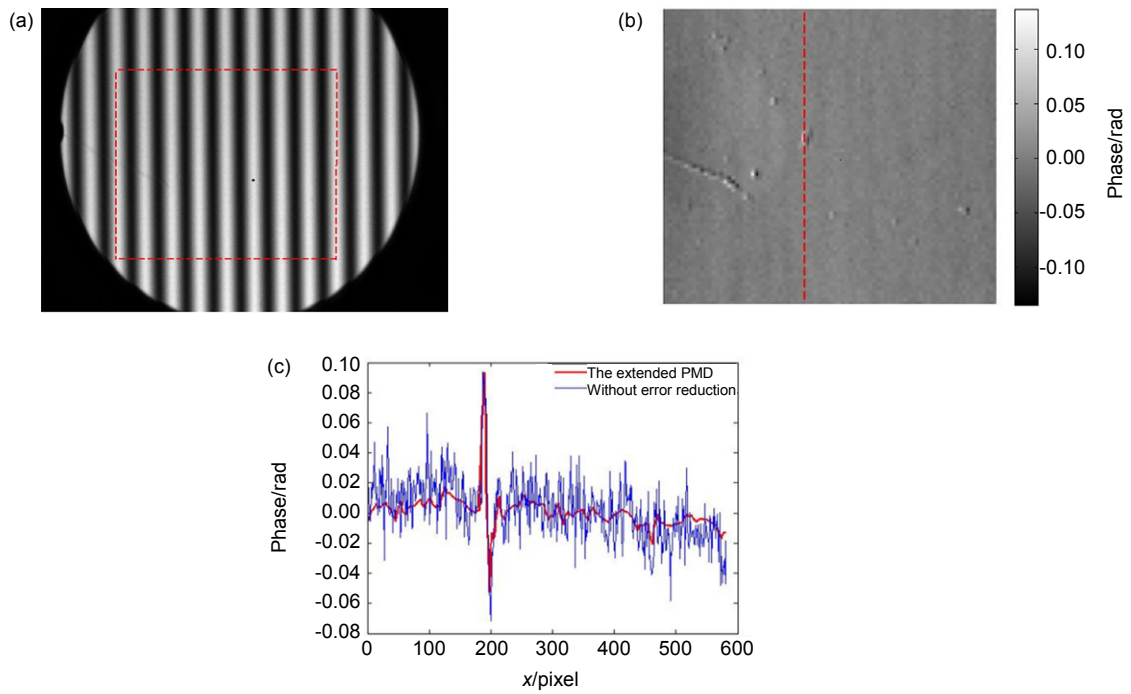

Fig. 10 The method based on wavelet de-noisings(extended PMD) in high reflectivity surface measurement. (a) The distorted fringe pattern. (b) The phase after using the method based on wavelet de-noising. (c) Comparison of the method based on wavelet de-noising and 6-step phase shifting method.

ment accuracy. Lastly, the phase, curvature and height error suppressing results using different error reduction methods are discussed. The method based on the wavelet de-noising shows better performance in improving the measurement accuracy of the low reflectivity specular surface in our experiment.

Acknowledgements

The authors wish to acknowledge the support by the National Nature Science Foundation of China (61421002, 61327004).

References

1 Knauer M C, Kaminski J, Hausler G. Phase measuring deflectometry: a new approach to measure specular free-form surfaces[J]. *Proceedings of SPIE*, 2004, **5457**: 366–376.

2 Song Lei, Yue Huimin, Kim H, *et al*. A study on carrier phase distortion in phase measuring deflectometry with non-telecentric imaging[J]. *Optics Express*, 2012, **20**(22): 24505–24515.

3 Yue Huimin, Wu Yuxiang, Zhao Biyu, *et al*. A carrier removal method in phase measuring deflectometry based on the analytical carrier phase description[J]. *Optics Express*, 2013, **21**(19): 21756–21765.

4 Jüptner W, Bothe T. Sub-nanometer resolution for the inspection of reflective surfaces using white light[J]. *Proceedings of SPIE*, 2009, **7405**: 740502.

5 Bothe T, Li Wansong, von Kopylow C, *et al*. High-resolution 3D shape measurement on specular surfaces by fringe reflection[J]. *Proceedings of SPIE*, 2004, **5457**: 411–422.

6 Skydan O A, Lalor M J, Burton D R. 3D shape measurement of automotive glass by using a fringe reflection technique[J]. *Measurement Science and Technology*, 2006, **18**(1): 106–114.

7 Zhang Song, Van Der Weide D, Oliver J. Superfast phase-shifting method for 3-D shape measurement[J]. *Optics Express*, 2010, **18**(9): 9684–9689.

8 Zhang Qican, Wu Zhiyun. A carrier removal method in Fourier transform profilometry with Zernike polynomials[J]. *Optics and Lasers in Engineering*, 2013, **51**(3): 253–260.

9 Notni G H, Notni G. Digital fringe projection in 3D shape measurement: an error analysis[J]. *Proceedings of SPIE*, 2003, **5144**: 372–380.

10 Liu Yong, Huang Dingfa, Jiang Yong. Flexible error-reduction method for shape measurement by temporal phase unwrapping: phase averaging method[J]. *Applied Optics*, 2012, **51**(21): 4945–4953.

11 Pan Bing, Kemao Qian, Huang Lei, *et al*. Phase error analysis and compensation for nonsinusoidal waveforms in phase-shifting digital fringe projection profilometry[J]. *Optics Letters*, 2009, **34**(4): 416–418.

12 Hoang T, Pan Bing, Nguyen D, *et al*. Generic gamma correction for accuracy enhancement in fringe-projection profilometry[J]. *Optics Letters*, 2010, **35**(12): 1992–1994.

13 Xiao Kaida, Fu Chenyang, Karatzas D, *et al*. Visual gamma correction for LCD displays[J]. *Displays*, 2011, **32**(1): 17–23.

14 Healey G E, Kondepudy R. Radiometric CCD camera calibration and noise estimation[J]. *IEEE Transactions on Pattern Analysis and Machine Intelligence*, 1994, **16**(3): 267–276.

15 Faraji H, MacLean W J. CCD noise removal in digital images[J]. *IEEE Transactions on Image Processing*, 2006, **15**(9): 2676–2685.

16 Wu Yuxiang, Yue Huimin, Ji Jingya, *et al*. Dynamic specular surface measurement based on color-encoded fringe reflection technique[J]. *Optical Engineering*, 2016, **55**(2): 024104.

17 Schmit J, Creath K. Extended averaging technique for derivation of error-compensating algorithms in phase-shifting interferometry[J]. *Appllied Optics*, 1995, **34**(19): 3610–3619.

18 Huntley J M, Saldner H O. Error-reduction methods for shape measurement by temporal phase unwrapping[J]. *Journal of the Optical Society of America A*, 1997, **14**(12): 3188–3196.

19 Ma Jun, Wang Zhaoyang, Vo M, *et al*. Wavelet selection in two-dimensional continuous wavelet transform technique for optical fringe pattern analysis[J]. *Journal of Optics*, 2012, **14**(6): 065403.

20 Huang Lei, Kemao Qian, Pan Bing, *et al*. Comparison of Fourier transform, windowed Fourier transform, and wavelet transform methods for phase extraction from a single fringe pattern in fringe projection profilometry[J]. *Optics and Lasers in Engineering*, 2010, **48**(2): 141–148.

21 Zhang Zibang, Zhong Jingang. Applicability analysis of wavelet-transform profilometry[J]. *Optics Express*, 2013, **21**(16): 18777–18796.

22 Chang S G, Yu Bin, Vetterli M. Adaptive wavelet thresholding for image denoising and compression[J]. *IEEE Transactions on Image Processing*, 2000, **9**(9): 1532–1546.

23 Nowak R D. Wavelet-based Rician noise removal for magnetic resonance imaging[J]. *IEEE Transactions on Image Processing*, 1999, **8**(10): 1408–1419.

24 Chen Yichun, Lin P C, Lee C M, *et al*. Iterative phase-shifting algorithm immune to random phase shifts and tilts[J]. *Applied Optics*, 2013, **52**(14): 3381–3386.

25 Messer S R, Agzarian J, Abbott D. Optimal wavelet denoising for phonocardiograms[J]. *Microelectronics Journal*, 2001, **32**(12): 931–941.